

Magnetic Control of the Non-Hermitian Skin Effect in Two-Dimensional Lattices

Stefano Longhi^{1,2,*}

¹*Dipartimento di Fisica, Politecnico di Milano, Piazza L. da Vinci 32, I-20133 Milano, Italy*

²*IFISC (UIB-CSIC), Instituto de Física Interdisciplinar y Sistemas Complejos, E-07122 Palma de Mallorca, Spain*

The non-Hermitian skin effect (NHSE) — the anomalous boundary accumulation of an extensive number of bulk modes — has emerged as a hallmark of non-Hermitian physics, with broad implications for transport, sensing, and topological classification. A central open question is how magnetic or synthetic gauge fields influence this boundary phenomenon. Here, we develop a theoretical framework for magnetic control of the NHSE along line boundaries in two-dimensional single-band lattices. Using a non-Hermitian extension of the anisotropic Harper–Hofstadter model as a representative example, we show that magnetic fields suppress the geometric skin effect in reciprocal models, whereas skin localization can persist in nonreciprocal systems. The analysis disentangles the interplay of flux, nonreciprocity, and boundary geometry, revealing that magnetic fields mitigate or suppress the NHSE through distinct physical mechanisms — such as bulk localization via Landau or Anderson physics, or the restoration of effective reciprocity. In particular, the geometry-dependent skin effect in reciprocal systems is found to be fragile against even weak magnetic fields.

I. INTRODUCTION

The non-Hermitian skin effect (NHSE) — the accumulation of an extensive number of bulk eigenstates at system boundaries — has emerged as a defining feature of non-Hermitian systems^{1–43}, with broad implications for condensed matter, photonics, acoustics, and engineered quantum platforms (for reviews, see^{22,26,28,29,32–34,38,43}). The NHSE reflects the breakdown of conventional bulk-boundary correspondence^{1,3,5} and underlies unconventional transport, enhanced sensing, and novel topological classifications. It was first identified in one-dimensional models with nonreciprocal (asymmetric) hopping^{1–3,5}, such as the Hatano–Nelson chain^{44–47}, and has since been generalized to higher-dimensional systems, reciprocal lattices, many-body, incoherent and nonlinear models (see, e.g.,^{24,25,35,48–79} and references therein). Several theoretical frameworks — including non-Bloch band theory, biorthogonal bulk-boundary correspondence, and real-space topological invariants — have provided a unified understanding of the NHSE by connecting spectral winding, boundary accumulation, and topological protection^{22,23,26,28,29,32–34,47}. Experimental demonstrations in photonic, acoustic, mechanical, topoelectrical, and ultracold atomic platforms^{15–17,20,21,25,27,31,35,36,80–82} have further established its generality and tunability.

Magnetic or synthetic gauge fields offer a natural mechanism to control the NHSE^{83–94}. Their effects, however, are highly system dependent, particularly in two-dimensional lattices where distinct types of NHSE and boundary dependencies arise²⁴. In nonreciprocal systems, magnetic fields can mitigate or suppress first-order NHSE by restoring Landau-level-like bulk states and shrinking the skin topological area, thereby reducing boundary accumulation^{83,84,91}. Similar suppression has been observed for pseudomagnetic fields engineered from spatially inhomogeneous gauge configurations⁹⁰. Conversely, magnetic fields can enhance or induce skin localization in other regimes: they stabilize second-

order skin modes by protecting line gaps in the complex spectrum⁸⁷, or drive field-induced transitions in spinful non-Hermitian systems^{92–94}. Moreover, the suppression of skin modes observed for weak magnetic fields and low-energy regimes associated with Landau localization⁸³ can decrease or disappear as the magnetic flux is increased⁸⁶. These contrasting behaviors illustrate the complex interplay between gauge fields and non-Hermitian topology, which remains far from fully understood. In particular, the distinctive role of gauge fields on skin states in nonreciprocal versus reciprocal models — the latter exhibiting the so-called geometric NHSE^{24,35,36} — remains poorly characterized.

In this work, we present a theoretical framework for analyzing the magnetic control of the NHSE in two-dimensional single-band lattices with strip geometries. Using a non-Hermitian extension of the anisotropic Harper–Hofstadter model^{90,95,96} as a representative example, we examine the interplay among flux, nonreciprocity, and boundary geometry. The results show that magnetic fields suppress the geometry-dependent skin effect in reciprocal systems, rendering it fragile even under weak flux, while skin localization in nonreciprocal systems is not universally suppressed. In the latter case, gauge-field-induced mixing of boundary modes qualitatively modifies the localization pattern and can mitigate, or in some regimes suppress, skin accumulation through Landau- or Anderson-type bulk localization. By contrast, in reciprocal systems the suppression of the geometry-dependent skin effect arises primarily from the field-induced restoration of effective reciprocity rather than bulk localization.

This study provides a coherent interpretation of how gauge fields influence boundary accumulation in reciprocal and nonreciprocal two-dimensional models, highlighting the fragility of the geometric NHSE in the presence of magnetic flux. The analysis builds upon and connects previous results across condensed-matter, photonic, and acoustic settings, contributing to the broader understanding of boundary phenomena in non-Hermitian

physics.

II. MODEL AND BASIC EQUATIONS

We consider a single-band two-dimensional lattice with one atom per unit cell. The wavefunction is denoted by $\psi(\mathbf{R})$, where \mathbf{R} labels the lattice sites. The sites are defined as

$$\mathbf{R} = n\mathbf{a}_X + m\mathbf{a}_Y = na_X\mathbf{u}_X + ma_Y\mathbf{u}_Y, \quad n, m \in \mathbb{Z}, \quad (1)$$

where $\mathbf{a}_X = a_X\mathbf{u}_X$ and $\mathbf{a}_Y = a_Y\mathbf{u}_Y$ are the primitive vectors of the Bravais lattice \mathcal{B} , forming an angle α with each other (Fig.1), and $\mathbf{u}_{X,Y}$ are the associated unit vectors. The system is subject to a uniform magnetic field B perpendicular to the crystal (X, Y) plane. We aim to investigate how the magnetic field controls NHSE localization toward a *rather arbitrary* edge direction x (first-order NHSE), forming an angle θ with the principal direction X . We remark that the direction x does not necessarily coincide with the X or Y axes of the primitive vectors. To this end, we consider a *strip geometry*: the lattice is infinite along the x direction (with periodic boundary conditions, x -PBC) and finite along y (with open boundary conditions, y -OBC). Eventually, y -PBC condition can be assumed along the y direction as well to relate the emergence of the NHSE toward the y edges, under y -OBC, with the point-gap topology of the reduced Hamiltonian, under y -PBC. The x axis is chosen such that a subset of sites of the Bravais lattice lies along it, as illustrated schematically in Fig.1. This condition is met provided that the ratio

$$\frac{a_X \sin \theta}{a_Y \sin(\alpha - \theta)} \equiv \frac{p}{q} \quad (2)$$

is rational, with p, q coprime integer numbers. The y axis is rotated relative to x by the same angle α between the primitive vectors.

To describe the effect of the magnetic field on the energy spectrum and eigenstate localization in the strip geometry, we adopt the Landau gauge in the (x, y) frame:

$$\mathbf{A}(\mathbf{r}) = (B \sin \alpha y, 0, 0), \quad (3)$$

where the obliquity factor $\sin \alpha$ in Eq.(3) accounts for the non-orthogonality of the x and y directions. The tight-binding eigenvalue equation reads

$$E\psi(\mathbf{R}) = \sum_{\delta} t(\delta) \exp(i\phi_{\mathbf{R}, \mathbf{R}+\delta}) \psi(\mathbf{R} + \delta), \quad (4)$$

where $\delta \in \mathcal{B}$, $t(\delta)$ is the hopping rate between sites \mathbf{R} and $\mathbf{R} + \delta$, and

$$\phi_{\mathbf{R}, \mathbf{R}+\delta} = 2\pi \int_{\mathbf{R}}^{\mathbf{R}+\delta} d\mathbf{r} \cdot \mathbf{A}(\mathbf{r}) \quad (5)$$

is the Peierls' phase (gauge phase) contribution to the hopping amplitude arising from the vector potential (we

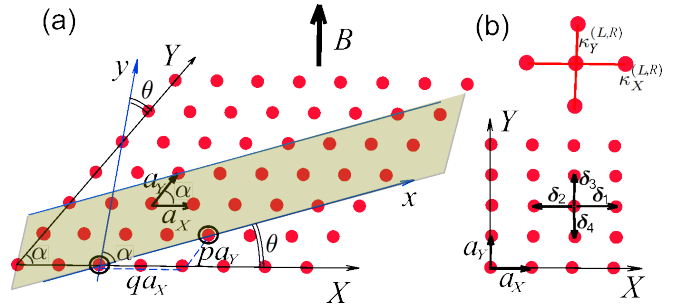


FIG. 1: (a) Schematic of a 2D crystal with a magnetic field B applied orthogonal to the crystal plane (X, Y) . $\mathbf{a}_X = a_X\mathbf{u}_X$ and $\mathbf{a}_Y = a_Y\mathbf{u}_Y$ are the primitive vectors of the Bravais lattice \mathcal{B} , forming an angle α with each other. We consider a strip geometry (shaded area) defined along the x and y directions, where the system is infinite along x (equivalently, periodic boundary conditions are imposed, x -PBC) and finite along y with open boundary conditions (y -OBC). The y axis is rotated relative to x by the same angle α between the primitive vectors, while the x axis is rotated by θ with respect to the principal axis X of the crystal. (b) Schematic of the non-Hermitian anisotropic Harper-Hofstadter model (rectangular lattice with nearest-neighbor hopping).

assume $h = e = 1$, i.e. a unit flux quantum). The integral on the right hand side of Eq.(5) is taken along the straight line connecting \mathbf{R} and $\mathbf{R} + \delta$. We indicate by $\mathcal{B}_H \in \mathcal{B}$ the subset of vectors of the Bravais lattice \mathcal{B} such that $t(\delta) \neq 0$, i.e. for which particle hopping can arise from site $\mathbf{R} + \delta$ to site \mathbf{R} . The lattice is *reciprocal* provided that, for any $\delta \in \mathcal{B}_H$, then also $-\delta \in \mathcal{B}_H$ and

$$|t(-\delta)| = |t(\delta)|. \quad (6)$$

If the additional condition $t(-\delta) = t^*(\delta)$ holds, then the lattice is also *Hermitian*.

To solve the eigenvalue equation (4) in the strip geometry, it is worth assuming the variable $\mathbf{R} = (x, y)$ as a continuous one. Owing to the Landau gauge (3), the Peierls' phase $\phi_{\mathbf{R}, \mathbf{R}+\delta}$ turns out to be a function of y solely, namely one has

$$\phi_{\mathbf{R}, \mathbf{R}+\delta} = 2\pi B y \sin \alpha (\delta_x + \delta_y \cos \alpha) + \theta_\delta \quad (7)$$

where we have set

$$\theta_\delta = \pi B \delta_y \sin \alpha (\delta_x + \delta_y \cos \alpha) \quad (8)$$

and $\delta = \delta_x\mathbf{u}_x + \delta_y\mathbf{u}_y$. Here, $\mathbf{u}_{x,y}$ are the unit vectors of the rotated directions x and y (Fig.1). Since the Peierls' phase depends only on y , under x -PBC we consider wavefunctions of the form

$$\psi(x, y) = \phi(y) e^{ik_x x}, \quad (9)$$

with k_x a constant quasi-momentum along the x -direction. Substitution of Eq.(9) into Eq.(4) yields the following difference equation for $\phi(y)$

$$E\phi(y) = \sum_{\delta_y} \tau_{\delta_y}(y) \phi(y + \delta_y) \quad (10)$$

where we have set

$$\tau_{\delta_y}(y) = \sum_{\delta_x} t(\boldsymbol{\delta}) \times \exp\{2\pi i B y \sin \alpha (\delta_x + \delta_y \cos \alpha) + i k_x \delta_x + i \theta_{\boldsymbol{\delta}}\}. \quad (11)$$

Since the vector $\boldsymbol{\delta} \in \mathcal{B}_H$ belongs to the Bravais lattice, there are two integers n_X and n_Y such that $\boldsymbol{\delta} = n_X a_X \mathbf{u}_X + n_Y a_Y \mathbf{u}_Y$, so that after some straightforward algebra one obtains

$$\delta_x = n_X a_X \frac{\sin(\alpha + \theta)}{\sin \alpha} + n_Y a_Y \frac{\sin \theta}{\sin \alpha} \quad (12)$$

$$\delta_y = -n_X a_X \frac{\sin \theta}{\sin \alpha} + n_Y a_Y \frac{\sin(\alpha - \theta)}{\sin \alpha}. \quad (13)$$

From Eqs.(2) and (13), one can write

$$\delta_y = a(-n_X p + n_Y q) \quad (14)$$

with

$$a \equiv a_X \frac{\sin \theta}{p \sin \alpha}.$$

This means that the spatial shifts δ_y , as $\boldsymbol{\delta}$ varies in \mathcal{B}_H , is an integer multiple than a , and thus Eq.(10) is formally analogous to the eigenvalue problem on a 1D lattice with lattice constant a . After letting $y = na$ and $\phi_n = \phi(y = na)$, Eq.(10) reads

$$E \phi_n = \sum_l \tau_l(n) \phi_{n+l} \equiv \sum_m \mathcal{H}_{n,m} \phi_m \quad (15)$$

where

$$\tau_l(n) = \sum_{\boldsymbol{\delta} | \delta_y = la} t(\boldsymbol{\delta}) \times \exp\{2\pi i B n a \sin \alpha (\delta_x + l a \cos \alpha) + i k_x \delta_x + i \theta_{\boldsymbol{\delta}}\} \quad (16)$$

is the effective hopping rates between sites distant la . Equations (15) and (16) represent an effective 1D lattice model in the y direction of the slab, described by the spatial Hamiltonian \mathcal{H} , and provide the starting point to investigate the skin localization of bulk modes toward the x -edge direction and the role of the magnetic field B in controlling skin localization.

III. MAGNETIC CONTROL OF NON-HERMITIAN SKIN EFFECT

Let us first consider the case $B = 0$, corresponding to the vanishing of Peierls' phases. The Bloch energy spectrum of the 2D lattice, under X -PBC and Y -PBC, is given by

$$E = H(\mathbf{k}) = \sum_{\boldsymbol{\delta} \in \mathcal{B}_N} t(\boldsymbol{\delta}) \exp(i \mathbf{k} \cdot \boldsymbol{\delta}). \quad (17)$$

The area covered by $H(\mathbf{k})$ on the complex plane, as \mathbf{k} spans the first Brillouin zone, is called the spectral area. A general result on the universality of the NHSE, stated in Ref.²⁴, is that the skin effect emerges under open boundary of generic geometry if and only if the spectral area is nonzero. This universal form of the skin effect can be partitioned into two classes: the nonreciprocal skin effect and the generalized reciprocal skin effect. The former arises quite generally in systems with nonreciprocal hopping and is characterized by nonvanishing currents, whereas the latter occurs in reciprocal models, with the geometry-dependent skin effect²⁴ being a characteristic example. This special type of generalized reciprocal NHSE exhibits the unique feature that there always exists at least one boundary geometry for which the skin effect is completely absent.

In the effective 1D model obtained in the strip geometry of Fig.1(a), in the absence of the magnetic field ($B = 0$) the hopping rates $\tau_l(n)$ do not depend on n and the effective 1D lattice defined by Eq.(15) displays discrete spatial invariance along y . The condition for the appearance of the NHSE under y -OBC, i.e. the localization of a macroscopic number of bulk modes toward the y edges of the strip, is that the energy spectrum E of Eq.(15), under y -PBC, shows a point-gap topology, i.e. it does not describe an open arc in complex energy plane. After letting $\phi_n = \exp(ik_y a n)$, the y -PBC energy spectrum reads

$$H_y(k_y) = \sum_l \tau_l \exp(ik_y a l). \quad (18)$$

Therefore the NHSE under y -OBC appears if and only if the curve $H_x(k_y)$ describes a closed loop with point gap topology, i.e. if for some base energy E_B the winding number^{12,22,29,32,33,47}

$$w(E_B) = \frac{1}{2\pi i} \int_0^{2\pi/a} dk_y \frac{d}{dk_y} \log \{H_y(k_y) - E_B\} \quad (19)$$

is nonvanishing. According to the general results of Ref.²⁴, for generic edge directions y the winding number is non-vanishing, for both reciprocal and non-reciprocal non-Hermitian lattices. A special form of reciprocal NHSE is the geometry-dependent skin effect that arises in certain reciprocal models: while the winding number w is non-vanishing for rather arbitrary y direction, and thus accumulation of skin modes is observed under y -OBC, for special directions y , corresponding to special symmetries of the model (such as mirror symmetries), the winding number vanishes and the skin effect is not observed²⁴.

When the magnetic field is turned on ($B \neq 0$), Eq. (16) shows that the hopping amplitudes $\tau_l(n)$ (for $l \neq 0$) and the on-site energy $\tau_0(n)$ in the effective one-dimensional Hamiltonian \mathcal{H} [Eq. (15)] become spatially inhomogeneous. As a result, discrete translational symmetry is generally broken: the magnetic field effectively introduces an incommensurate disorder into the lattice, which can strongly affect skin localization of the eigenstates

of \mathcal{H} under y -OBC. Owing to the breakdown of translational invariance, various forms of winding numbers defined in real space have been proposed to characterize the emergence of skin states under y -OBC^{23,47,97}. For instance, for a given base energy E_B , one may consider the polar decomposition of the shifted Hamiltonian $(\mathcal{H} - E_B) = \mathcal{Q}\mathcal{P}$, where the unitary factor \mathcal{Q} captures the spectral winding in real space and thus provides a direct diagnostic of the NHSE. The winding number $w(E_B)$ can be introduced as^{23,97}

$$w(E_B) = \frac{1}{L} \text{Tr} (\mathcal{Q}^\dagger [\mathcal{Q}, \mathcal{X}]) \quad (20)$$

where L is the lattice size and \mathcal{X} is the position operator. Such a definition of the winding number $w(E_B)$ reduces to Eq. (19) in the translationally invariant limit $B = 0$. Another way to verify the suppression of the skin effect via winding numbers is to introduce an additional gauge phase Φ in the y -PBC and evaluate the winding number $w(E_B)$ as⁴⁷

$$w(E_B) = \frac{1}{2\pi i} \int_0^{2\pi} d\Phi \frac{d}{d\Phi} \ln \det(\mathcal{H} - E_B),$$

which is quantized, with $w(E_B) = 0$ signaling the disappearance of the NHSE due to bulk localization of the eigenstates. In practice, numerical detection of the NHSE is often more straightforward by comparing the spectra under y -OBC and y -PBC. In the absence of the NHSE, the two spectra coincide in the thermodynamic limit ($L \rightarrow \infty$), apart from a finite, L -independent set of edge states under y -OBC. In the Hermitian limit, these boundary states correspond to the familiar chiral edge modes connecting bands with different Chern numbers. By contrast, in the presence of the NHSE, the spectra under y -OBC and y -PBC are markedly different. In the following, the appearance of the NHSE will be probed using this spectral comparison, together with the mean spatial distribution of eigenvectors of \mathcal{H} under y -OBC.

To summarize, the above analysis indicates that magnetic fields can generally control the skin effect, in close analogy with lattice models subject to incommensurate disorder⁹¹. This argument, however, does not resolve the distinct responses of reciprocal and nonreciprocal models to magnetic fields, nor does it clarify the fate of the geometry-dependent skin effect in reciprocal lattices. To disentangle these mechanisms in a controlled setting, the next section introduces a non-Hermitian extension of the anisotropic Harper–Hofstadter model^{95,96}, which provides a minimal and paradigmatic framework for exploring magnetic control of the NHSE in two-dimensional quantum Hall systems.

IV. MAGNETIC CONTROL OF THE SKIN EFFECT IN THE NON-HERMITIAN HARPER-HOFSTADTER MODEL

We consider a non-Hermitian extension of the Harper–Hofstadter model^{90,95,96}, a paradigmatic model of two-

dimensional quantum Hall physics⁹⁵. This framework is directly relevant to a variety of experimental platforms, including photonic crystals, topoelectric circuits, and ultracold atoms, where synthetic magnetic fields and nonreciprocal couplings can be engineered. Specifically, we focus on a rectangular lattice ($\alpha = \pi/2$) with generally anisotropic and nonreciprocal nearest-neighbor hopping, defined by the set $\mathcal{B}_H = \{\delta_1, \delta_2, \delta_3, \delta_4\}$, with

$$\delta_1 = a_X \mathbf{u}_X, \delta_2 = -\delta_1, \delta_3 = a_Y \mathbf{u}_Y, \delta_4 = -\delta_3 \quad (21)$$

and

$$t(\delta_1) = \kappa_X^{(L)}, t(\delta_2) = \kappa_X^{(R)}, t(\delta_3) = \kappa_Y^{(L)}, t(\delta_4) = \kappa_Y^{(R)} \quad (22)$$

[see Fig.1(b)]. The rotation angle θ of the x direction with respect to the principal crystal axis X is assumed to satisfy the constraint (2), i.e.

$$\tan\theta = \frac{p a_Y}{q a_X} \quad (23)$$

where p, q are two irreducible (coprime) integers. After letting $a = (a_X/p) \sin\theta = (a_Y/q) \cos\theta$, the effective one-dimensional eigenvalue equation in the y direction is obtained by specializing Eqs.(15) and (16) using Eqs.(21) and (22). One obtains

$$E\phi_n = \tau_p(n)\phi_{n+p} + \tau_q(n)\phi_{n+q} + \tau_{-p}(n)\phi_{n-p} + \tau_{-q}(n)\phi_{n-q} \quad (24)$$

where we have set

$$\tau_p(n) = \kappa_X^{(R)} \exp(-2\pi i \alpha_x n + i\sigma_p)$$

$$\tau_{-p}(n) = \kappa_X^{(L)} \exp(2\pi i \alpha_x n + i\sigma_{-p})$$

$$\tau_q(n) = \kappa_Y^{(L)} \exp(2\pi i \alpha_y n + i\sigma_q)$$

$$\tau_{-q}(n) = \kappa_Y^{(R)} \exp(-2\pi i \alpha_y n + i\sigma_{-q})$$

and

$$\alpha_x = B a a_X \cos\theta, \alpha_y = B a a_Y \sin\theta \quad (25)$$

$$\sigma_p = -k_x a_X \cos\theta - \pi B a_X a p \cos\theta \quad (26)$$

$$\sigma_{-p} = k_x a_X \cos\theta - \pi B a_X a p \cos\theta \quad (27)$$

$$\sigma_q = k_x a_Y \sin\theta + \pi B a_Y a q \sin\theta \quad (28)$$

$$\sigma_{-q} = -k_x a_Y \sin\theta + \pi B a_Y a q \sin\theta \quad (29)$$

To illustrate the above framework, two representative cases are analyzed in detail, after which a general discussion of the results is presented.

A. Non-reciprocal lattices

The first case corresponds to a nonreciprocal model, namely a two-dimensional extension of the Hatano–Nelson model^{44,45,47}, obtained by setting

$$\kappa_X^{(L)} = J_X \exp(h_X), \quad \kappa_X^{(R)} = J_X \exp(-h_X), \quad (30)$$

$$\kappa_Y^{(L)} = J_Y \exp(h_Y), \quad \kappa_Y^{(R)} = J_Y \exp(-h_Y), \quad (31)$$

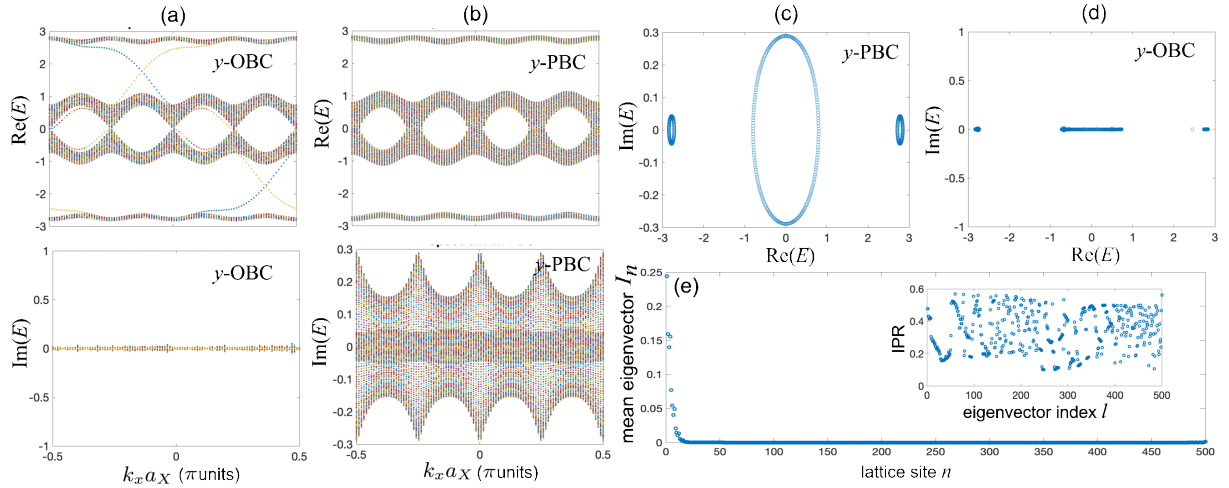


FIG. 2: Effect of a rational magnetic flux on the energy spectrum and skin localization for the non-reciprocal Harper-Hofstadter model in a slab geometry [Eq.(32)]. Parameter values are $h_X = 0$, $h_Y = 0.2$, $J_X = J_Y = 1$ and magnetic flux $\Phi = \alpha_x = \pi/2$. Lattice size in the y direction is $L = 500$. (a,b) Energy spectrum versus quasi-momentum $k_x a_X$ under y -OBC [panels (a)] and y -PBC [panels (b)]. Real and imaginary parts of E are shown in the upper and lower panels, respectively. The curves in the gaps in panel (a) correspond to non-Hermitian extension of usual chiral edge states in the 2D quantum Hall model. (c,d) Energy spectrum in complex energy plane for $k_x a_X = 0$ and for y -PBC [panel (c)] and y -OBC [panel (d)]. (e) Mean eigenvector distribution I_n under y -OBC, clearly showing the persistence of the NHSE. The inset in (e) shows the IPR of the L eigenstates under y -OBC.

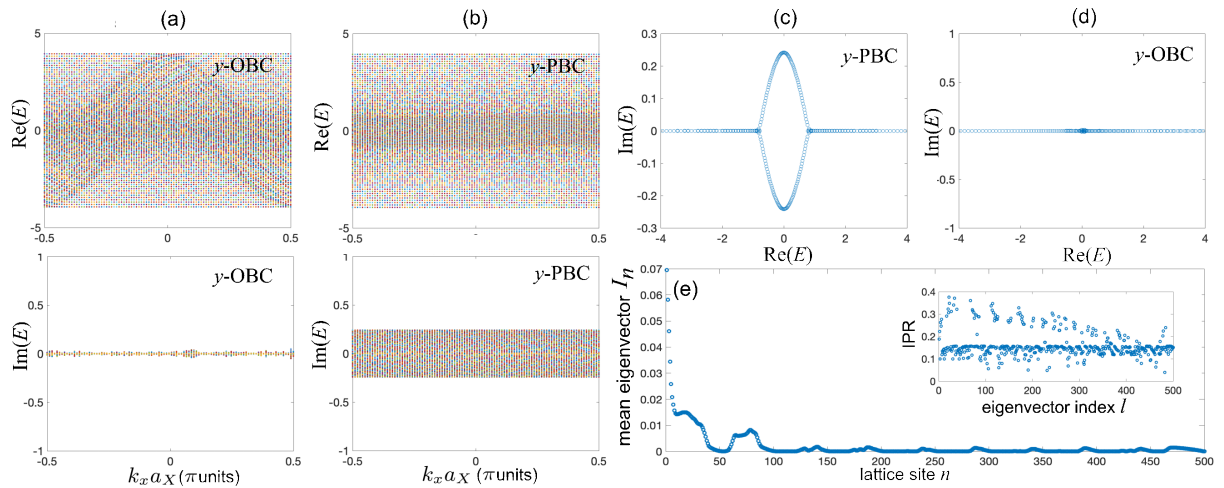


FIG. 3: Same as Fig.2, but for a weak magnetic flux $\Phi = \pi/50$. Note that the skin area in panel (c) is reduced as compared to the case of Fig.2(c), and the corresponding mean eigenvector distribution I_n in (e) tends to spread toward the bulk owing to the competing Landau localization.

where J_X , J_Y , h_X , and h_Y are real parameters describing the horizontal/vertical hopping amplitudes and the associated imaginary gauge fields, respectively. This model exhibits the NHSE under OBC for essentially arbitrary boundary orientation x . As a representative example, let us consider $\theta = 0$, i.e., a slab geometry with $x = X$ and $y = Y$. In this case one has $p = 0$, $q = 1$, and Eq. (24) reduces to

$$E\phi_n = J_Y \exp(h_Y) \phi_{n+1} + J_Y \exp(-h_Y) \phi_{n-1} + 2J_X \cos(2\pi\alpha_x n + k_x a_X - ih_X) \phi_n. \quad (32)$$

where $\alpha_x = Ba_X a_Y \equiv \Phi$ is the magnetic flux in each plaquette of the rectangular lattice. Equation (32) represents a non-Hermitian extension of the Aubry–André–Harper model, which has been the subject of extensive recent investigations^{98–110}. In the absence of a magnetic field ($B = 0$), Eq. (32) reduces to the clean Hatano–Nelson model, which exhibits the NHSE under y -OBC for any $h_Y \neq 0$. When a magnetic field is present, one must distinguish between the cases of rational and irrational magnetic flux α_x .

In the *rational case*, Eq. (32) describes a superlattice with nonreciprocal hopping. The corresponding energy

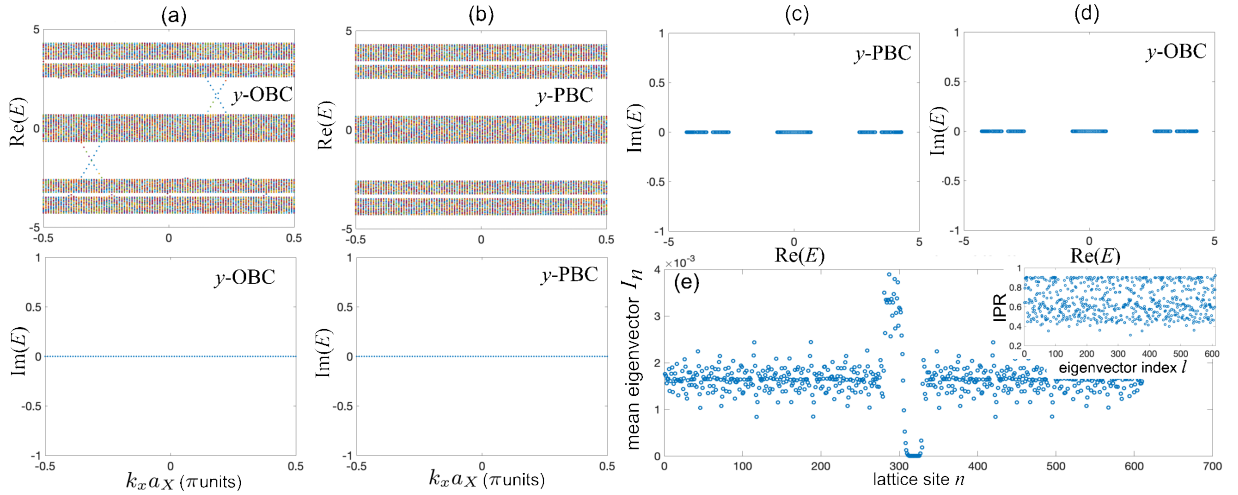


FIG. 4: Same as Fig. 2, but for an irrational magnetic flux $\Phi = (\sqrt{5} - 1)/2$. Other parameter values are $J_X = 2$, $J_Y = 1$, $h_X = 0$ and $h_Y = 0.2$. In numerical simulations, the inverse of the golden ratio has been approximated by the rational number $\alpha \simeq 377/610$, i.e. ratio of Fibonacci numbers, and a lattice of size $L = 610$ has been assumed. The energy spectrum is the same for y -PBC and y -OBC [apart for chiral edge states under y -OBC, visible in panel (a)], the eigenstates are bulk localized via Anderson localization and the NHSE is fully suppressed.

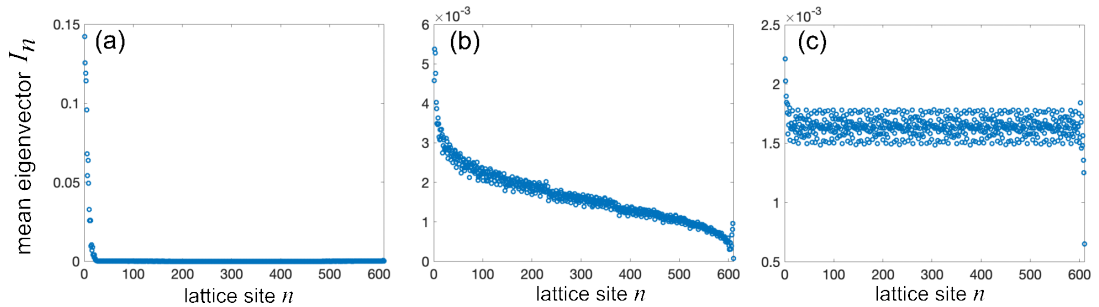


FIG. 5: Suppression of the skin effect in the isotropic Harper-Hofstadter model ($J_X = J_Y = 1$) under an irrational magnetic flux ($\Phi = (\sqrt{5} - 1)/2$) by the application of non-reciprocal hopping parameter h_X in the X direction. The panels show the numerically-computed behavior of the mean eigenvector distribution I_n of the Hamiltonian under y -OBC for $h_Y = 0.2$, quasi-momentum $k_x a_X = 0$, and for a few increasing values of h_X : (a) $h_X = 0$, (b) $h_X = h_Y = 0.2$, and (c) $h_X = 0.3$.

spectrum under y -PBC consists of a set of closed loops in the complex plane, which differs substantially from the spectrum under y -OBC¹¹¹—beyond the usual appearance of chiral edge states. As a result, the NHSE cannot be completely suppressed by the magnetic field for rational flux. An illustrative example is shown in Fig. 2 for $\Phi = \pi/2$. Figures 2(a) and 2(b) display the numerically computed energy spectrum (real and imaginary parts in the upper and lower panels, respectively) as a function of the quasi-momentum $k_x a_X$ in a lattice of size $L = 500$, for y -OBC [Fig. 2(a)] and y -PBC [Fig. 2(b)] with parameter values $J_X = J_Y = 1$, $h_X = 0$, and $h_Y = 0.2$. The spectra in the complex energy plane at $k_x a_X = 0$ are shown in Figs. 2(c) and 2(d), corresponding to y -PBC and y -OBC, respectively. Notably, the y -PBC spectrum is distinct than the y -OBC spectrum and consists of closed loops that enclose a finite area, which is a clear signature of the NHSE. This feature is further confirmed in Fig. 2(e), where the numerically computed mean eigen-

vector distribution I_n is plotted:

$$I_n = \frac{1}{L} \sum_{l=1}^L |\phi_n^{(l)}|^2, \quad (33)$$

with $\phi_n^{(l)}$ denoting the normalized l -th eigenvector of Eq. (32) under y -OBC. The inset shows the inverse participation ratio (IPR) of the L eigenstates, defined as $\text{IPR}_l = \sum_n |\phi_n^{(l)}|^4$. For extended states, the IPR takes small values scaling as $\sim 1/L$, while for localized states it remains finite and independent of system size L . As one can see, the eigenvectors are localized and preferentially accumulate near the left lattice edge, indicating the persistence of skin localization. However, for small magnetic flux Φ , the skin topological area—namely, the area enclosed by the closed spectral loops—shrinks, and the eigenstates show a tendency toward bulk localization. This crossover is associated with bulk Landau-type localization in the low-energy regime of the model^{83,91} which

competes with skin localization, as illustrated in Fig. 3.

In the *irrational case*, the eigenstates of Eq. (32) under y -PBC undergo a localization–delocalization transition at the critical point

$$|h_Y| + \ln \left| \frac{J_Y}{J_X} \right| - |h_X| = 0 \quad (34)$$

which has been derived in previous works (see e.g.¹⁰⁶). In fact, in the Hermitian limit $h_X = h_Y = 0$ Eq. (32) reduces to the usual Aubry-André model, which displays a localization-delocalization transition at $|J_X| = |J_Y|$ with a Lyapunov exponent (inverse of localization length) given by $\lambda = \ln |J_X/J_Y|$ in the localized phase $|J_X/J_Y| > 1$. The addition of non-reciprocal hopping via the imaginary gauge field h_Y tends to delocalize the eigenstates, i.e. reduce the Lyapunov exponent, while the imaginary phase h_X in the incommensurate potential tends to localize the eigenstates, i.e. to increase the Lyapunov exponent. Overall, the critical point of the transition, corresponding to vanishing of the Lyapunov exponent, is provided by Eq.(34). In particular, bulk Anderson localization occurs whenever

$$|h_Y| + \ln \left| \frac{J_Y}{J_X} \right| - |h_X| < 0, \quad (35)$$

indicating that in this regime the NHSE is completely suppressed by the magnetic field and the eigenstates become localized in the bulk. As a representative example, consider reciprocal hopping along the X direction ($h_X = 0$), where the incommensurate potential in Eq.(32) is real. In this case, the above condition shows that magnetic flux can eliminate the NHSE provided $J_X > J_Y$ and the nonreciprocal hopping parameter in the Y direction satisfies $|h_Y| < \ln |J_X/J_Y|$. An illustrative example of magnetic suppression of skin localization in this regime is presented in Fig. 4, where the magnetic flux $\Phi = (\sqrt{5} - 1)/2$ is the inverse golden mean and the parameter values satisfy Eq. (35). As evidenced by the behavior of the IPR [inset of Fig. 4(e)], all eigenstates under y -OBC are localized. However, unlike the skin modes, they are no longer confined to the boundary; instead, they are localized in the bulk at various lattice sites, yielding an almost uniform mean eigenvector distribution [Fig. 4(e)].

A special case is provided by the isotropic Harper–Hofstadter model with $J_X = J_Y$. The preceding analysis indicates that the NHSE cannot be suppressed by the magnetic field when $h_X = 0$. Indeed, in the Hermitian limit ($h_Y = 0$), Eq. (32) reduces to the Harper equation, whose eigenstates are critical, being neither exponentially localized nor fully extended. As soon as a small nonreciprocity $h_Y \neq 0$ is applied to the vertical hopping rates, all states become skin modes localized at one edge under y -OBC. However, increasing h_X , i.e., introducing nonreciprocity along the x direction with PBC, allows condition (35) to be satisfied, and the NHSE can then be suppressed by the magnetic field. Remarkably, nonreciprocity along the periodic x direction can inhibit the emergence of skin localization along the transverse y direction with OBC. This counterintuitive effect is illustrated in Fig. 5.

B. Reciprocal lattices

The second case corresponds to non-Hermitian lattices with reciprocal hopping, $\kappa_X^{(L)} = \kappa_X^{(R)} \equiv \kappa_X$ and $\kappa_Y^{(L)} = \kappa_Y^{(R)} \equiv \kappa_Y$, which display the geometry-dependent NHSE²⁴ in the absence of the magnetic field. In fact, for $B = 0$ the dispersion curve of the lattice band reads

$$E(k_X, k_Y) = 2\kappa_X \cos(k_X a) + 2\kappa_Y \cos(k_Y a_Y) \quad (36)$$

which displays in complex E plane a non-vanishing spectral area for generic non-Hermitian (yet reciprocal) hopping amplitudes κ_X, κ_Y . For an edge along a rather arbitrary y direction, one expects skin localization of bulk modes toward the edge, with the exception when y is one of the two principal directions X or Y of the Bravais lattice, i.e. at the cut angles $\theta = 0, \pi/2$. In the following analysis, we assume a cut angle θ satisfying Eq.(23) with $p = q = 1$, i.e. along the main diagonal of the rectangle forming the primitive cell of the lattice. In this case, the eigenvalue equation (15) takes the form

$$E\phi_n = W_n^{(L)}\phi_{n+1} + W_{n-1}^{(R)}\phi_{n-1} \quad (37)$$

where we have set

$$W_n^{(L)} = \kappa_X \exp(-2\pi i \alpha_x n - ik_x a_X \cos \theta - i\pi \Phi \cos^2 \theta) + \kappa_Y \exp(2\pi i \alpha_y n + ik_x a_Y \sin \theta + i\pi \Phi \sin^2 \theta) \quad (38)$$

$$W_n^{(R)} = \kappa_X \exp(2\pi i \alpha_x n + ik_x a_X \cos \theta + i\pi \Phi \cos^2 \theta) + \kappa_Y \exp(-2\pi i \alpha_y n - ik_x a_Y \sin \theta - i\pi \Phi \sin^2 \theta), \quad (39)$$

and $\alpha_x = \Phi \cos^2 \theta$, $\alpha_y = \Phi \sin^2 \theta$ and $\Phi = Ba_X a_Y$. Therefore, in the effective 1D lattice model [Eq.(37)] the magnetic field introduces a spatial modulation of the ef-

fective left and right hopping rates, $W_n^{(L,R)}$. In the absence of the magnetic field ($B = 0$), the lattice is homo-

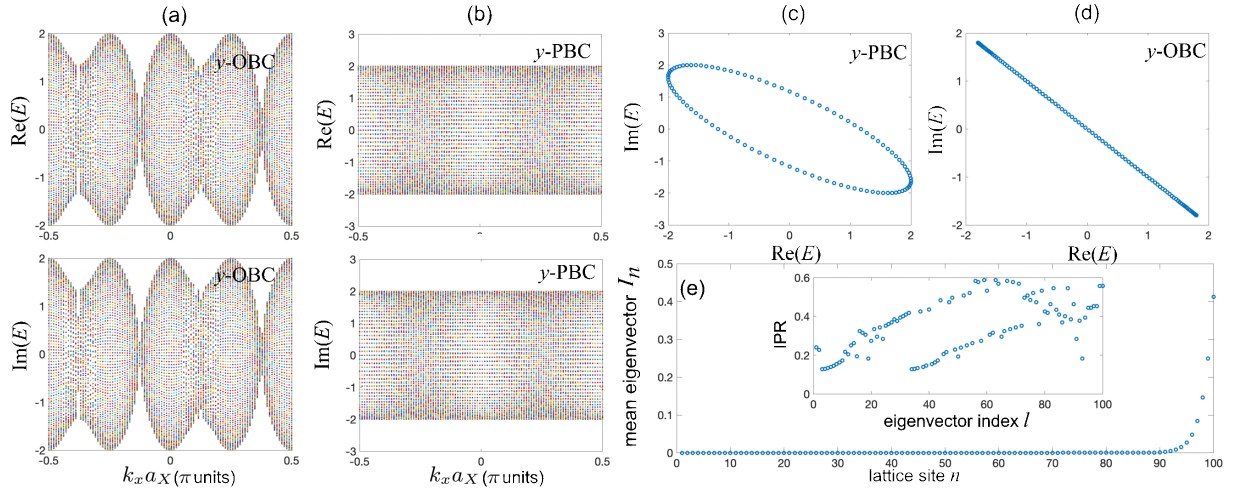


FIG. 6: Geometry-dependent NHSE in the reciprocal Harper-Hofstadter model in a slab geometry. (a,b) Energy spectrum versus quasi-momentum $k_x a$ under y -OBC [panels (a)] and y -PBC [panels (b)], for $a_x = a_y = \sqrt{2}a$, corresponding to $\theta = \pi/4$ and $\alpha_x = \alpha_y = \Phi/2$, and for parameter values $\kappa_X = 1$, $\kappa_Y = i$ and $\Phi = 0$. Lattice size in the x direction is $L = 100$. Real and imaginary parts of E are shown in the upper and lower panels, respectively. (c,d) Energy spectrum in complex energy plane for $k_x a = 2\pi/5$ and for y -PBC [panel (c)] and y -OBC [panel (d)]. (e) Mean eigenvector distribution I_n under y -OBC, clearly showing the presence of the NHSE. The inset in (e) shows the IPR of the L eigenstates under y -OBC.

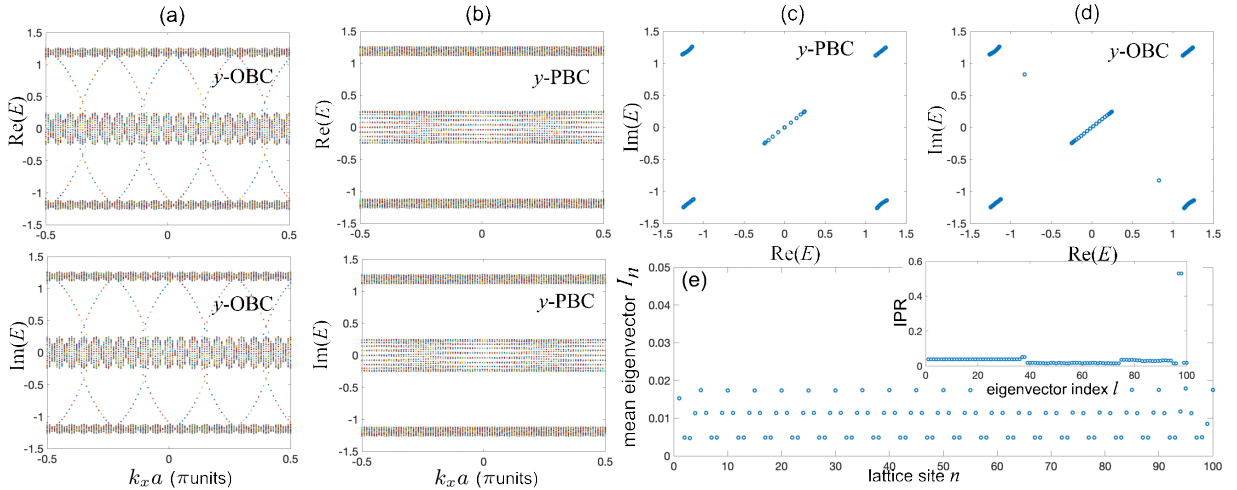


FIG. 7: Suppression of the geometry-dependent NHSE in the reciprocal Harper-Hofstadter model under a weak magnetic field. Parameter values are as Fig.6 except for a magnetic flux $\Phi = 1/5$.

geneous with hopping rates

$$\begin{aligned} W^{(L)} &= \kappa_X \exp(-ik_x a_X \cos \theta) + \kappa_Y \exp(ik_x a_Y \sin \theta) \\ W^{(R)} &= \kappa_X \exp(ik_x a_X \cos \theta) + \kappa_Y \exp(-ik_x a_Y \sin \theta). \end{aligned}$$

In a non-Hermitian yet reciprocal lattice, i.e. when $\kappa_X \neq \kappa_X^*$ and/or $\kappa_Y \neq \kappa_Y^*$, for rather arbitrary quasi-momentum k_x one has $|W^{(L)}| \neq |W^{(R)}|$, indicating the appearance of the NHSE. This is shown, as an example, in Fig.6. When the magnetic field is turned on, the hopping rates are modulated, with $|W_n^{(L)}| > |W_n^{(R)}|$ in some sites and $|W_n^{(L)}| < |W_n^{(R)}|$ in the other sites. Specifically,

one has

$$\frac{|W_n^{(R)}(E)|^2}{|W_n^{(L)}(E)|^2} = \frac{|\kappa_X|^2 + |\kappa_Y|^2 + 2|\kappa_X||\kappa_Y|\cos(\omega_n + \rho)}{|\kappa_X|^2 + |\kappa_Y|^2 + 2|\kappa_X||\kappa_Y|\cos(\omega_n - \rho)} \quad (40)$$

where we have set $\omega_n = \pi\Phi(2n + 1) + k_x a / (\sin \theta \cos \theta)$ and ρ is the phase of $\kappa_X \kappa_Y^*$. This relation indicates that, while the model (37) is locally non-reciprocal with unbalanced left/right hopping rates for $\rho \neq 0, \pi$, i.e. $|W_n^{(R)}|/|W_n^{(L)}| \neq 1$, the modulation induced by the magnetic field tends to restore *global reciprocity*^{41,112} favoring the mitigation or even the suppression of the NHSE. For example, if the magnetic flux in each plaquette $\Phi = Ba_x a_y$ is chosen such that $\Phi = \pi/2$, then $\omega_n \bmod$

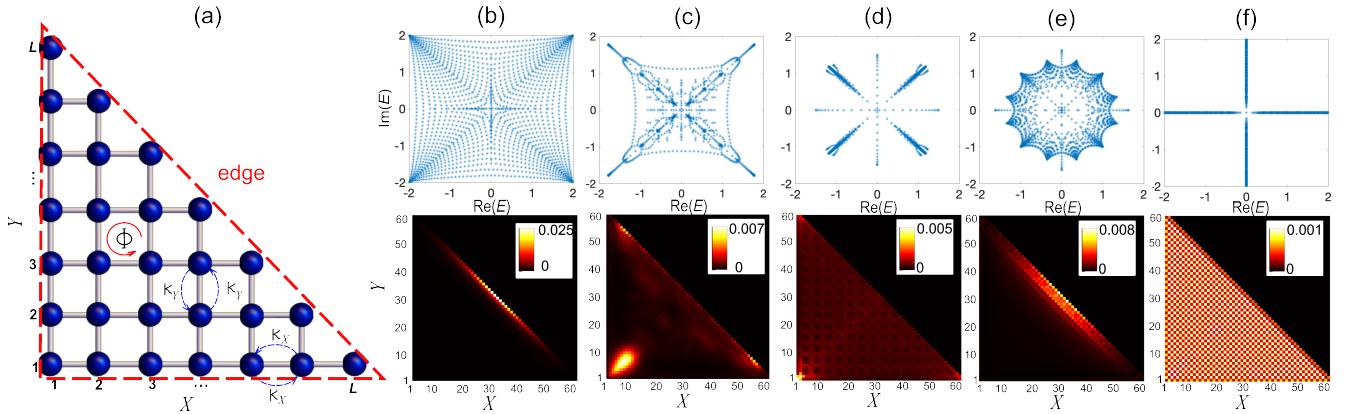


FIG. 8: (a) Schematic of a 2D square lattice ($a_X = a_Y$) with reciprocal hopping amplitudes κ_X in the horizontal X direction and κ_Y in the vertical Y direction. OBC are assumed along a triangular contour (dashed red curve). The total number of sites in the lattice with OBC is $N = L(L + 1)/2$. Parameter values used in the numerical simulations are $\kappa_X = 1$, $\kappa_Y = i$ and $L = 60$. (b-f) Energy spectrum (upper panels) and mean eigenvector distribution $I_{X,Y}$ on a pseudocolor map (lower plots) for a few increasing values of the magnetic flux $\Phi = a_X a_Y B$: (b) $\Phi = 0$; (c) $\Phi = \pi/20$; (d) $\Phi = \pi/4$; (e) $\Phi = \pi/3$; (f) $\Phi = \pi/2$.

2π takes only two opposite values and thus the ratio in Eq.(40) alternates between two values λ and $1/\lambda$, indicating perfect balance between left and right hopping on average and suggesting full suppression of the NHSE. More generally, as demonstrated in the Appendix A a small magnetic flux, or an irrational magnetic flux, can suppress the skin effect. An illustrative example of magnetic suppression of geometry-dependent skin effect for a weak magnetic flux is shown in Fig.7.

C. Discussion

It should be emphasized that the present analysis has been carried out in a strip geometry invariant along the x direction [Fig. 1(a)] and in Landau gauge, where periodic boundary conditions allow for an analytic reduction to an effective one-dimensional model. This framework provides clear insight into the distinct mechanisms by which magnetic fields control skin localization. Nevertheless, introducing boundaries along the x direction, or more generally considering polygonal geometries, can modify the routes to boundary localization, potentially giving rise to edge- or corner-localized modes controlled by flux. As an illustrative example, consider the reciprocal model of Sec. IV.B with a square lattice ($a_X = a_Y$, $\theta = \pi/2$) terminated by a triangular boundary, as shown in Fig. 8(a). The numerically computed mean eigenvector distribution $I_{X,Y}$ and the corresponding energy spectrum for increasing values of the magnetic flux $\Phi = B a_X a_Y$ are displayed in Figs. 8(b-f). For vanishing flux, skin localization is observed along the diagonal edge of the triangle, a manifestation of the geometry-dependent skin effect²⁴ [Fig. 8(b)]. For a weak magnetic flux, the boundary accumulation is mitigated and replaced by a tendency toward bulk and corner localization [Figs. 8(c-d)]. As the magnetic flux is increased, according to the anal-

ysis of Sec. IV.B and Appendix A, the suppression of the skin effect depends sensitively on the value of the magnetic flux Φ , since global reciprocity is only partially restored. For instance, at $\Phi = \pi/3$ the suppression remains incomplete [Fig. 8(d)], while at $\Phi = \pi/2$ the NHSE is fully suppressed [Fig. 8(f)]. These results exemplify how boundary geometry and magnetic fields can cooperate to reshape localization patterns beyond the strip geometry. While a general universal theory for arbitrary polygonal boundaries remains an open challenge, the triangular-lattice example highlights the versatility of magnetic fields as a means of tailoring boundary phenomena in non-Hermitian systems. It also provides a natural bridge to the broader implications and perspectives discussed in the Conclusions.

V. CONCLUSIONS

In this work, we have presented a theoretical analysis of magnetic control of the non-Hermitian skin effect in two-dimensional single-band lattices with strip geometries. By examining a non-Hermitian extension of the anisotropic Harper–Hofstadter model, we clarified the respective roles of flux, nonreciprocity, and boundary geometry. Our results show that magnetic fields suppress the geometry-dependent NHSE in reciprocal systems, rendering it fragile even under weak flux, whereas skin localization in nonreciprocal systems is more robust but can nevertheless be mitigated or suppressed through gauge-field-induced bulk localization mechanisms. Two distinct routes by which magnetic fields influence boundary accumulation have been identified: restoration of effective reciprocity in reciprocal models and Landau- or Anderson-type localization in nonreciprocal ones.

These findings shed light on the mechanisms underlying the interplay between gauge fields and non-Hermitian

topology, helping to clarify how magnetic flux affects boundary accumulation in different regimes. While our analysis focuses on a representative single-band model, the general trends identified here may be relevant to a broader class of non-Hermitian systems. Several directions for further study emerge. Extensions to multiband systems, higher-order skin effects, or models with spin-orbit coupling may reveal additional mechanisms of magnetic control. The interplay between gauge fields and many-body or nonlinear non-Hermitian systems represents another timely challenge, with potential to uncover new forms of collective localization.

Appendix A: Magnetic suppression of geometry-dependent skin effect

In this Appendix it is shown that application of a weak magnetic field, or more generally of an irrational magnetic flux, to the reciprocal non-Hermitian model of Sec.IV.B suppresses the geometry-dependent skin effect. To this aim, let us consider the eigenvalue equation (37), given in the main text

$$E\phi_n = W_n^{(L)}\phi_{n+1} + W_{n-1}^{(R)}\phi_{n-1} \quad (\text{A1})$$

and assume OBC, i.e. $\phi_0 = \phi_{L+1} = 0$, where L is the lattice size. As discussed in the main text, an extensive NHSE arises in the absence of the magnetic flux for a rather generic value of the quasi-momentum k_x , i.e. there is a macroscopic piling of the eigenstates ϕ_n to one boundary. To prove that a non-vanishing magnetic field can suppresses the NHSE, let us first introduce the gauge transformation

$$\phi_n = \xi_n \exp(i\pi\alpha_x n^2 + i\sigma_x n - i\pi\alpha_x n) \quad (\text{A2})$$

where we have set $\sigma_x \equiv k_x a_X \cos\theta + \pi\Phi \cos^2\theta$. Then, using Eqs.(38) and (39), the eigenvalue equation (A1) takes the form

$$E\xi_n = \tilde{W}_n^{(L)}\xi_{n+1} + \tilde{W}_{n-1}^{(R)}\xi_{n-1} \quad (\text{A3})$$

with the OBC $\xi_0 = \xi_{L+1} = 0$, where we have set

$$\tilde{W}_n^{(L)} = \kappa_X + \kappa_Y \exp(i\omega_n), \quad \tilde{W}_n^{(R)} = \kappa_X + \kappa_Y \exp(-i\omega_n) \quad (\text{A4})$$

and

$$\omega_n = \pi\Phi(2n+1) + \frac{k_x a}{\sin\theta \cos\theta}. \quad (\text{A5})$$

Let us assume that the magnetic flux in each plaquette, $\Phi = Ba_X a_Y$, is weak or close to an irrational number, such that there exists a *large integer* q such that $\tilde{W}_{n+q}^{(L,R)} \simeq \tilde{W}_n^{(L,R)}$. Let us then write Eq.(A3) in transfer-matrix form

$$\begin{pmatrix} \xi_{n+1} \\ \xi_n \end{pmatrix} = \mathcal{M}_n(E) \begin{pmatrix} \xi_n \\ \xi_{n-1} \end{pmatrix} \quad (\text{A6})$$

with transfer matrix

$$\mathcal{M}_n(E) = \begin{pmatrix} \frac{E}{\tilde{W}_n^{(L)}} & -\frac{\tilde{W}_{n-1}^{(R)}}{\tilde{W}_n^{(L)}} \\ 1 & 0 \end{pmatrix}. \quad (\text{A7})$$

Over Nq sites one has

$$\begin{pmatrix} \xi_{Nq+1} \\ \xi_{Nq} \end{pmatrix} = \mathcal{S}^N(E) \begin{pmatrix} \xi_1 \\ \xi_0 \end{pmatrix} \quad (\text{A8})$$

where we have set

$$\mathcal{S}(E) = \mathcal{M}_q(E)\mathcal{M}_{q-1}(E)\dots\mathcal{M}_1(E). \quad (\text{A9})$$

Under OBC in a lattice comprising $L = Nq$ sites, $\xi_0 = \xi_{Nq+1} = 0$ and thus from Eq.(A) one obtains

$$(\mathcal{S}^N(E))_{1,1} = 0 \quad (\text{A10})$$

and

$$\xi_{Nq} = (\mathcal{S}^N(E))_{2,1} \xi_1. \quad (\text{A11})$$

The first condition, Eq.(A10), determines the set of Nq allowed energies E (energy spectrum), whereas Eq.(A11) indicates that the ratio $|\phi_{Nq}/\phi_1| = |\xi_{Nq}/\xi_1|$ scales with N as $|(\mathcal{S}^N(E))_{2,1}|$. The NHSE arises whenever for almost all energies E in the spectrum $(\mathcal{S}^N(E))_{2,1}$ diverges or vanishes exponentially as $N \rightarrow \infty$. Indicating by $\lambda_{1,2}(E)$ the two eigenvalues of the matrix $\mathcal{S}(E)$ and by \mathcal{T} the matrix of eigenvectors, taking into account that

$$\mathcal{S}^N(E) = \mathcal{T} \begin{pmatrix} \lambda_1^N(E) & 0 \\ 0 & \lambda_2^N(E) \end{pmatrix} \mathcal{T}^{-1} \quad (\text{A12})$$

the condition (A10) implies that, when E is in the spectrum, then $|\lambda_1(E)| = |\lambda_2(E)|$ for almost any energy E , whereas Eq.(A11) shows that the NHSE arises whenever at least one of the two eigenvalues has modulus different than one for almost any energy E in the spectrum. As we prove below, for any E one has $|\det \mathcal{S}(E)| = |\lambda_1(E)\lambda_2(E)| = 1$, and since $|\lambda_1(E)| = |\lambda_2(E)|$ for almost any energy in the spectrum, one concludes $|\lambda_1(E)| = |\lambda_2(E)| = 1$ for almost any energy in the spectrum and thus the NHSE effect is absent.

We now prove that $|\det \mathcal{S}(E)| = 1$. To this aim, let us notice that

$$\begin{aligned} |\det \mathcal{S}(E)|^2 &= |\det \mathcal{M}_q|^2 |\det \mathcal{M}_{q-1}|^2 \dots |\det \mathcal{M}_1|^2 = \\ &= \frac{\prod_{n=1}^q |\tilde{W}_n^{(R)}(E)|^2}{\prod_{n=1}^q |\tilde{W}_n^{(L)}(E)|^2} = \\ &= \frac{\prod_{n=1}^q |W_n^{(R)}(E)|^2}{\prod_{n=1}^q |W_n^{(L)}(E)|^2} \end{aligned} \quad (\text{A13})$$

where we used the cyclic property $W_n^{(L,R)}(E) = W_{n+q}^{(L,R)}(E)$. Physically, the condition $|\det \mathcal{S}(E)| = 1$ corresponds to global reciprocity of the system. From the

explicit form of $\tilde{W}_n^{(L,R)}(E)$ given by Eq.(A4), one obtains

$$|\det \mathcal{S}(E)|^2 = \frac{\prod_{n=1}^q (|\kappa_X|^2 + |\kappa_Y|^2 + 2|\kappa_X||\kappa_Y| \cos(\omega_n + \rho))}{\prod_{n=1}^q (|\kappa_X|^2 + |\kappa_Y|^2 + 2|\kappa_X||\kappa_Y| \cos(\omega_n - \rho))} \quad (\text{A14})$$

where ρ is the phase of $\kappa_X \kappa_Y^*$. From Eq.(A14) one obtains

$$\begin{aligned} \ln |\det \mathcal{S}(E)|^2 = & \sum_{n=1}^q \ln \{ |\kappa_X|^2 + |\kappa_Y|^2 + 2|\kappa_X||\kappa_Y| \cos(\omega_n + \rho) \} \\ & - \sum_{n=1}^q \ln \{ |\kappa_X|^2 + |\kappa_Y|^2 + 2|\kappa_X||\kappa_Y| \cos(\omega_n - \rho) \}. \end{aligned} \quad (\text{A15})$$

In the large q limit, as n varies from 1 to q the phase ω_n mod 2π uniformly fills the interval $(0, 2\pi)$, so that one can write

$$\begin{aligned} \sum_{n=1}^q \ln \{ |\kappa_X|^2 + |\kappa_Y|^2 + 2|\kappa_X||\kappa_Y| \cos(\omega_n \pm \rho) \} \simeq \\ \frac{q}{2\pi} \int_0^{2\pi} d\omega \ln \{ |\kappa_X|^2 + |\kappa_Y|^2 + 2|\kappa_X||\kappa_Y| \cos(\omega \pm \rho) \} \end{aligned} \quad (\text{A16})$$

Clearly, the integral on the right hand side of Eq.(A16) is independent of ρ , and thus the two sums on the right hand side of Eq.(A15) are the same, yielding $\ln |\det \mathcal{S}(E)|^2 = 0$, i.e. $|\det \mathcal{S}(E)| = 1$.

Finally, we mention that for rational flux $\Phi = p/q$ with relatively small q the condition $|\det \mathcal{S}(E)| = 1$ cannot be rather generally strictly satisfied, i.e. global reciprocity restoration is imperfect, and the skin effect is only partly mitigated. On the other hand, in some special conditions one exactly has $|\det \mathcal{S}(E)| = 1$ even for small q , for example for a flux $\Phi = p/q = 1/2$, one has exactly $|\det \mathcal{S}(E)| = 1$, leading to perfect washing out of the NHSE.

* stefano.longhi@polimi.it

¹ S. Yao and Z. Wang, Edge states and topological invariants of non-Hermitian systems, *Phys. Rev. Lett.* **121**, 086803 (2019).

² V. M. Martinez Alvarez, J. E. Barrios Vargas, and L. E. F. Foa Torres, Non-Hermitian robust edge states in one dimension: Anomalous localization and eigenspace condensation at exceptional points, *Phys. Rev. B* **97**, 121401 (2018).

³ C.H. Lee and R. Thomale, Anatomy of skin modes and topology in non-Hermitian systems, *Phys. Rev. B* **99**, 201103 (2019).

⁴ K. Yokomizo and S. Murakami, Non-Bloch band theory of non-Hermitian systems, *Phys. Rev. Lett.* **123**, 066404 (2019).

⁵ F. K. Kunst, E. Edvardsson, J. C. Budich, and E. J. Bergholtz, Biorthogonal bulk-boundary correspondence in non-Hermitian systems, *Phys. Rev. Lett.* **121**, 026808 (2018).

⁶ S. Longhi, Probing non-Hermitian skin effect and non-Bloch phase transitions, *Phys. Rev. Research* **1**, 023013 (2019).

⁷ L. E. F. Foa Torres, Perspective on topological states of non-Hermitian lattices, *Journal of Physics: Materials* **3**, 014002 (2019).

⁸ F. Song, S. Yao, and Z. Wang, Non-Hermitian topological invariants in real space, *Phys. Rev. Lett.* **123**, 246801 (2019).

⁹ F. Song, S. Yao, and Z. Wang, Non-Hermitian Skin Effect and Chiral Damping in Open Quantum Systems, *Phys. Rev. Lett.* **123**, 170401 (2019).

¹⁰ S. Longhi, Unraveling the non-Hermitian skin effect in dissipative systems, *Phys. Rev. B* **102**, 201103(R) (2020).

¹¹ D.S. Borgnia, A.J. Kruchkov, and R.-J. Slager, Non-Hermitian Boundary Modes and Topology, *Phys. Rev. Lett.* **124**, 056802 (2020).

¹² N. Okuma, K. Kawabata, K. Shiozaki, and M. Sato, Topological Origin of Non-Hermitian Skin Effects, *Phys. Rev. Lett.* **124**, 086801 (2020).

¹³ K. Zhang, Z. Yang, and C. Fang, Correspondence between winding numbers and skin modes in non-Hermitian systems, *Phys. Rev. Lett.* **125**, 126402 (2020).

¹⁴ L. Li, C. H. Lee, S. Mu, and J. Gong, Critical non-Hermitian skin effect, *Nature Commun.* **11**, 5491 (2020).

¹⁵ T. Helbig, T. Hofmann, S. Imhof, M. Abdelghany, T. Kiessling, L. W. Molenkamp, C. H. Lee, A. Szameit, M. Greiter, and R. Thomale, Generalized bulk-boundary correspondence in non-Hermitian topoelectrical circuits, *Nature Phys.* **16**, 747 (2020).

¹⁶ L. Xiao, T. Deng, K. Wang, G. Zhu, Z. Wang, W. Yi, and P. Xue, Non-Hermitian bulk-boundary correspondence in quantum dynamics, *Nature Phys.* **16**, 761 (2020).

¹⁷ S. Weidemann, M. Kremer, T. Helbig, T. Hofmann, A. Stegmaier, M. Greiter, R. Thomale, and A. Szameit, Topological funneling of light, *Science* **368**, 311 (2020).

¹⁸ Y. Yi and Z. Yang, Non-Hermitian Skin Modes Induced by On-Site Dissipations and Chiral Tunneling Effect, *Phys. Rev. Lett.* **125**, 186802 (2020).

¹⁹ Z. Yang, K. Zhang, C. Fang, and J. Hu, Non-Hermitian Bulk-Boundary Correspondence and Auxiliary Generalized Brillouin Zone Theory, *Phys. Rev. Lett.* **125**, 226402 (2020).

- ²⁰ A. Ghatak, M. Brandenbourger, J. van Wezel, and C. Coulais, Observation of non-Hermitian topology and its bulk-edge correspondence in an active mechanical metamaterial, *Proc Nat. Acad. Sci.* **117**, 29561 (2020).
- ²¹ K. Wang, T. Li, L. Xiao, Y. Han, W. Yi, and P. Xue, Detecting non-Bloch topological invariants in quantum dynamics, *Phys. Rev. Lett.* **127**, 270602 (2021).
- ²² E.J. Bergholtz, J. C. Budich, and F.K. Kunst, Exceptional topology of non-Hermitian systems, *Rev. Mod. Phys.* **93**, 015005 (2021).
- ²³ J. Claes and T. L. Hughes, Skin effect and winding number in disordered non-Hermitian systems, *Phys. Rev. B* **103**, L140201 (2021).
- ²⁴ K. Zhang, Z. Yang, and C. Fang, Universal non-Hermitian skin effect in two and higher dimensions, *Nat. Commun.* **13**, 2496 (2022).
- ²⁵ X. Zhang, Y. Tian, J.H. Jiang, M.H. Lu, and Y.F. Chen, Observation of higher-order non-Hermitian skin effect, *Nature Commun.* **12**, 5377 (2021).
- ²⁶ H. Wang, X. Zhang, J. Hua, D. Lei, M. Lu, and Y. Chen, Topological physics of non-Hermitian optics and photonics: a review, *J. Opt.* **23**, 123001 (2021).
- ²⁷ L. Zhang, Y. Yang, Y. Ge, Y. Guan, Q. Chen, Q. Yan, F. Chen, R. Xi, Y. Li, D. Jia, S. Yuan, H. Sun, H. Chen, and B. Zhang, Acoustic non-Hermitian skin effect from twisted winding topology, *Nature Commun.* **12**, 6297 (2021).
- ²⁸ K. Ding, C. Fang, and M. Guancong, Non-Hermitian topology and exceptional-point geometries, *Nat. Rev. Phys.* **4**, 745 (2022).
- ²⁹ X. Zhang, T. Zhang, M.-H. Lu, and Y.-F. Chen, A review on non-Hermitian skin effect, *Advances in Physics: X* **7**, 2109431 (2022).
- ³⁰ S. Longhi, Self-Healing of Non-Hermitian Topological Skin Modes, *Phys. Rev. Lett.* **128**, 157601 (2022).
- ³¹ Q. Liang, D. Xie, Z. Dong, H. Li, H. Li, B. Gadway, W. Yi, and B. Yan, Observation of Non-Hermitian Skin Effect and Topology in Ultracold Atoms, *Phys. Rev. Lett.* **129**, 070401 (2022).
- ³² N. Okuma and M. Sato, Non-Hermitian Topological Phenomena: A Review, *Annual Review of Condensed Matter Physics* **14** (2023).
- ³³ R. Lin, T. Tai, L. Li, and C.-H. Lee, Topological Non-Hermitian skin effect, *Front. Phys.* **18**, 53605 (2023).
- ³⁴ A. Banerjee, R. Sarkar, S. Dey, and A. Narayan, Non-Hermitian topological phases: principles and prospects, *J. Phys.: Cond. Matter* **35**, 333001 (2023).
- ³⁵ Q. Zhou, J. Wu, Z. Pu, J. Lu, X. Huang, W. Deng, M. Ke, and Z. Liu, Observation of geometry-dependent skin effect in non-Hermitian phononic crystals with exceptional points, *Nature Commun.* **14**, 4569 (2023).
- ³⁶ W. Wang, M. Hu, X. Wang, G. Ma, and K. Ding, Experimental realization of geometry-dependent skin effect in a reciprocal two-dimensional lattice, *Phys. Rev. Lett.* **131**, 207201 (2023).
- ³⁷ K. Shimomura and M. Sato, General Criterion for Non-Hermitian Skin Effects and Application: Fock Space Skin Effects in Many-Body Systems, *Phys. Rev. Lett.* **133**, 136502 (2024).
- ³⁸ H. Wang, J. Zhong, and S. Fan, Non-Hermitian photonic band winding and skin effects: a tutorial, *Adv. Opt. Photonics* **16**, 659 (2024).
- ³⁹ T. Yoshida, S.-B. Zhang, T. Neupert, and N. Kawakami, Non-Hermitian Mott Skin Effect, *Phys. Rev. Lett.* **133**, 076502 (2024).
- ⁴⁰ H.-Y. Wang, F. Song, and Z. Wang, Amoeba Formulation of Non-Bloch Band Theory in Arbitrary Dimensions, *Phys. Rev. X* **14**, 021011 (2024).
- ⁴¹ S. Longhi, Erratic non-Hermitian skin localization, *Phys. Rev. Lett.* **134**, 196302 (2025).
- ⁴² S. Kaneshiro and R. Peters, Symplectic-amoebe formulation of the non-Bloch band theory for one-dimensional two-band systems, *Phys. Rev. B* **112**, 075408 (2025).
- ⁴³ J.T. Gohsrich, A. Banerjee, and F.K. Kunst, The non-Hermitian skin effect: A perspective, *EPL* **150**, 60001 (2025).
- ⁴⁴ N. Hatano and D. R. Nelson, Localization transitions in non-Hermitian quantum mechanics, *Phys. Rev. Lett.* **77**, 570 (1996).
- ⁴⁵ N. Hatano and D. R. Nelson, Vortex pinning and non-Hermitian quantum mechanics, *Phys. Rev. B* **56**, 8651 (1997).
- ⁴⁶ S. Longhi, D. Gatti, and G. Della Valle, Robust light transport in non-Hermitian photonic lattices, *Sci. Rep.* **5**, 13376 (2015).
- ⁴⁷ Z. Gong, Y. Ashida, K. Kawabata, K. Takasan, S. Higashikawa, and M. Ueda, Topological phases of non-Hermitian systems, *Phys. Rev. X* **8**, 031079 (2018).
- ⁴⁸ C. H. Lee, L. Li, and J. Gong, Hybrid higher-order skin-topological modes in nonreciprocal systems, *Phys. Rev. Lett.* **123**, 016805 (2019).
- ⁴⁹ R. Okugawa, R. Takahashi, and K. Yokomizo, Second-order topological non-Hermitian skin effects, *Phys. Rev. B* **102**, 241202 (2020).
- ⁵⁰ K. Kawabata, M. Sato, and K. Shiozaki, Higher-order non-Hermitian skin effect, *Phys. Rev. B* **102**, 205118 (2020).
- ⁵¹ Y. Fu, J. Hu, and S. Wan, Non-Hermitian second-order skin and topological modes, *Phys. Rev. B* **103**, 045420 (2021).
- ⁵² Y. Li, C. Liang, C. Wang, C. Lu, and Y. C. Liu, Gain-loss-induced hybrid skin-topological effect, *Phys. Rev. Lett.* **128**, 223903 (2022).
- ⁵³ W. Zhu and J. Gong, Hybrid skin-topological modes without asymmetric couplings, *Phys. Rev. B* **106**, 035425 (2022).
- ⁵⁴ R. Hamazaki, K. Kawabata, and M. Ueda, Non-Hermitian Many-Body Localization, *Phys. Rev. Lett.* **123**, 090603 (2019).
- ⁵⁵ S. Mu, C. H. Lee, L. Li, and J. Gong, Emergent Fermi surface in a many-body non-Hermitian fermionic chain, *Phys. Rev. B* **102**, 081115 (2020).
- ⁵⁶ S. B. Zhang, M. M. Denner, T. Bzdusek, M. A. Sentef, and T. Neupert, Symmetry breaking and spectral structure of the interacting Hatano-Nelson model, *Phys. Rev. B* **106**, L121102 (2022).
- ⁵⁷ F. Alsallom, L. Herviou, O. V. Yazyev, and M. Brzeziska, Fate of the non-Hermitian skin effect in many-body fermionic systems, *Phys. Rev. Res.* **4**, 033122 (2022).
- ⁵⁸ B. Dora and C. P. Moca, Full counting statistics in the many-body Hatano-Nelson model, *Phys. Rev. B* **106**, 235125 (2022).
- ⁵⁹ T. Yoshida, K. Kudo, and Y. Hatsugai, Non-Hermitian fractional quantum Hall states, *Sci. Rep.* **9**, 16895 (2019).
- ⁶⁰ Y. N. Wang, W. L. You, and G. Sun, Quantum criticality in interacting bosonic Kitaev-Hubbard models, *Phys. Rev. A* **106**, 053315 (2022).
- ⁶¹ T. Yoshida and Y. Hatsugai, Reduction of one-

- dimensional non-Hermitian point-gap topology by interactions, *Phys. Rev. B* **106**, 205147 (2022).
- ⁶² W. Zhang, F. Di, H. Yuan, H. Wang, X. Zheng, L. He, H. Sun, and X. Zhang, Observation of non-Hermitian aggregation effects induced by strong interactions, *Phys. Rev. B* **105**, 195131 (2022).
- ⁶³ K. Kawabata, K. Shiozaki, and S. Ryu, Many-body topology of non-Hermitian systems, *Phys. Rev. B* **105**, 165137 (2022).
- ⁶⁴ T. Yoshida, Real-space dynamical mean field theory study of non-Hermitian skin effect for correlated systems: Analysis based on pseudospectrum, *Phys. Rev. B* **103**, 125145 (2021).
- ⁶⁵ S. Longhi, Phase transitions and bunching of correlated particles in a non-Hermitian quasicrystal, *Phys. Rev. B* **108**, 075121 (2023).
- ⁶⁶ S. Longhi, Spectral Structure and Doublon Dissociation in the Two-Particle Non-Hermitian Hubbard Model, *Ann. Phys.* **535**, 2300291 (2023).
- ⁶⁷ P. Brighi and A. Nunnenkamp, Nonreciprocal dynamics and the non-Hermitian skin effect of repulsively bound pairs, *Phys. Rev. A* **110**, L020201 (2024).
- ⁶⁸ J. Gliozzi, G. De Tomasi, and T. L. Hughes, Many-Body Non-Hermitian Skin Effect for Multipoles, *Phys. Rev. Lett.* **133**, 136503 (2024).
- ⁶⁹ S. Longhi, Incoherent non-Hermitian skin effect in photonic quantum walks, *Light: Sci. & App.* **13**, 95 (2024).
- ⁷⁰ R. Shen, F. Qin, J.-Y. Desaulles, Z. Papic, and C.-H. Lee, Enhanced Many-Body Quantum Scars from the Non-Hermitian Fock Skin Effect, *Phys. Rev. Lett.* **133**, 216601 (2024).
- ⁷¹ Y. Qin, C.-H. Lee, and L. Li, Dynamical suppression of many-body non-Hermitian skin effect in anyonic systems, *Commun. Phys.* **8**, 18 (2025).
- ⁷² C. Yuce, Nonlinear non-Hermitian skin effect, *Phys. Lett. A* **408**, 127484 (2021).
- ⁷³ M. Ezawa, Dynamical nonlinear higher-order non-Hermitian skin effects and topological trap-skin phase, *Phys. Rev. B* **105**, 125421 (2022).
- ⁷⁴ Z.-X. Zhang, J. Cao, J.-Q. Li, Y. Zhang, S. Liu, S. Zhang, and H.-F. Wang, Topological skin modes and intensity amplification in a nonlinear non-Hermitian lattice, *Phys. Rev. B* **108**, 125402 (2023).
- ⁷⁵ I. Komis, Z.H. Musslimani, and K.G. Makris, Skin solitons, *Opt. Lett.* **48**, 6525 (2023).
- ⁷⁶ B. Many Manda, R. Carretero-Gonzalez, P.G. Kevrekidis, and V. Achilleos, Skin modes in a nonlinear Hatano-Nelson model, *Phys. Rev. B* **109**, 094308 (2024).
- ⁷⁷ J. Veenstra, O. Gamayun, X. Guo, A. Sarvi, C.V. Meinersen, and C. Coullais, Non-reciprocal topological solitons in active metamaterials, *Nature* **627**, 528 (2024).
- ⁷⁸ S. Longhi, Modulational instability and dynamical growth blockade in the nonlinear Hatano-Nelson model, *Adv. Phys. Res.* **4**, 2400154 (2025).
- ⁷⁹ S. Wang, B. Wang, C. Liu, C. Qin, L. Zhao, W. Liu, S. Longhi, and P. Lu, Nonlinear Non-Hermitian Skin Effect and Skin Solitons in Temporal Photonic Feedforward Lattices, *Phys. Rev. Lett.* **134**, 243805 (2025).
- ⁸⁰ J.-X. Zhong, P. F. de Castro, T. Lu, J. Kim, M. Oudich, J. Ji, L. Shi, K. Chen, J. Lu, Y. Jing, and W. A. Benalcazar, Higher-order non-Hermitian skin effect in an acoustic lattice, *J. Acoust. Soc. Am.* **153**, 1423?1431 (2023).
- ⁸¹ J. X. Zhong, P. Fittipaldi de Castro, T. Lu, J. Kim, M. Oudich, J. Ji, L. Shi, K. Chen, J. Lu, Y. Jing, and W. A. Benalcazar, Higher-order skin effect and its observation in an acoustic kagome lattice, *Phys. Rev. B* **111**, 014314 (2025).
- ⁸² J.-X. Zhong, J. Kim, K. Chen, J. Lu, K. Ding, and Y. Jing, Experimentally probing non-Hermitian spectral transition and eigenstate skewness, arXiv:2501.08160 [cond-mat.mes-hall], (2025).
- ⁸³ M. Lu, X. X. Zhang, and M. Franz, Magnetic suppression of non-Hermitian skin effects, *Phys. Rev. Lett.* **127**, 256402 (2021).
- ⁸⁴ K. Shao, Z. T. Cai, H. Geng, W. Chen, and D. Y. Xing, Cyclotron quantization and mirror-time transition on nonreciprocal lattices, *Phys. Rev. B* **106**, L081402 (2022).
- ⁸⁵ K. Deng and B. Flebus, Non-Hermitian skin effect in magnetic systems, *Phys. Rev. B* **105**, L180406 (2022).
- ⁸⁶ M. M. Denner and F. Schindler, Magnetic flux response of non-Hermitian topological phases, *SciPost Phys.* **14**, 107 (2023).
- ⁸⁷ C.-A. Li, B. Trauzettel, T. Neupert, and S.-B. Zhang, Enhancement of second-order non-Hermitian skin effect by magnetic fields, *Phys. Rev. Lett.* **131**, 116601 (2023).
- ⁸⁸ Q. Wang, C. Zhu, X. Zheng, H. Xue, B. Zhang, and Y. D. Chong, Continuum of bound states in a non-Hermitian model, *Phys. Rev. Lett.* **130**, 103602 (2023).
- ⁸⁹ Q. Lin, W. Yi, and P. Xue, Manipulating directional flow in a two-dimensional photonic quantum walk under a synthetic magnetic field, *Nat. Commun.* **14**, 6283 (2023).
- ⁹⁰ H. T. Teo, S. Mandal, Y. Long, H. Xue, and B. Zhang, Pseudomagnetic suppression of non-Hermitian skin effect, *Science Bulletin* **69**, 1667 (2024).
- ⁹¹ C. Xu, Z. Guan, and H. Xu, Controllable suppression of non-Hermitian skin effects, *Phys. Rev. B* **111**, 024201 (2025).
- ⁹² W. Zhang, Y. Hu, H. Zhang, X. Liu, G. Veronis, Y. Shen, Y. Huang, W. Luo, and A. Alù, Skin effect in non-Hermitian systems with spin, arXiv:2408.07406 (2024).
- ⁹³ M. Sanahal, S. Panda, and S. Nandy, Gauge field induced skin effect in spinful non-Hermitian systems, *Phys. Rev. B* **112**, 125149 (2025).
- ⁹⁴ Y. Li, J.-H. Zhang, Y. Kou, L.-T. Xiao, S.-T. Jia, L. Li, and F. Mei, Observation of gauge field induced non-Hermitian helical spin skin effects, arXiv:2504.18063 (2025).
- ⁹⁵ D. R. Hofstadter, Energy levels and wave functions of Bloch electrons in rational and irrational magnetic fields, *Phys. Rev. B* **14**, 2239(1976).
- ⁹⁶ M. N. Chernodub and S. Ouvry, Fractal energy carpets in non-Hermitian Hofstadter quantum mechanics, *Phys. Rev. E* **92**, 042102 (2015).
- ⁹⁷ R. Sarkar, S. S. Hegde, and A. Narayan, Interplay of disorder and point-gap topology: Chiral modes, localization, and non-Hermitian Anderson skin effect in one dimension, *Phys. Rev. B* **106**, 014207 (2022).
- ⁹⁸ A. Jazaeri and I.I. Satija, Localization transition in incommensurate non-Hermitian systems, *Phys. Rev. E* **63**, 036222 (2001).
- ⁹⁹ S. Longhi, Topological phase transition in non-Hermitian quasicrystals, *Phys. Rev. Lett.* **122**, 237601 (2019).
- ¹⁰⁰ H. Jiang, L. J. Lang, C. Yang., S. L. Zhu, and S. Chen, Interplay of non-hermitian skin effects and anderson localization in nonreciprocal quasiperiodic lattices, *Phys. Rev. B* **100**, 054301 (2019).
- ¹⁰¹ S. Longhi, Metal-insulator phase transition in a non-

- Hermitian Aubry-Andre-Harper model, *Phys. Rev. B* **100**, 125157 (2019).
- ¹⁰² T. Liu, H. Guo, Y. Pu, and S. Longhi, Generalized Aubry-Andre self-duality and mobility edges in non-Hermitian quasiperiodic lattices, *Phys. Rev. B* **102**, 024205 (2020).
- ¹⁰³ Q.-B. Zeng, Y.-B. Yang, and Y. Xu, Topological phases in non-Hermitian Aubry-Andre-Harper models, *Phys. Rev. B* **101**, 020201(R) (2020).
- ¹⁰⁴ Q.-B. Zeng and Y. Xu, Winding numbers and generalized mobility edges in non-Hermitian systems, *Phys. Rev. Research* **2**, 033052 (2020).
- ¹⁰⁵ S. Longhi, Phase transitions in a non-Hermitian Aubry-André-Harper model, *Phys. Rev. B* **103**, 054203 (2021).
- ¹⁰⁶ Y. Liu, Q. Zhou, and S. Chen, Localization transition, spectrum structure and winding numbers for one-dimensional non-Hermitian quasicrystals, *Phys. Rev. B* **104**, 024201 (2021).
- ¹⁰⁷ S. Longhi, Non-Hermitian Maryland model, *Phys. Rev. B* **103**, 224206 (2021).
- ¹⁰⁸ S. Weidemann, M. Kremer, S. Longhi, and A. Szameit, Topological triple phase transition in non-Hermitian Floquet quasicrystals *Nature* **601**, 354 (2022).
- ¹⁰⁹ Q. Lin, T. Li, L. Xiao, K. Wang, W. Yi, and P. Xue, Topological phase transitions and mobility edges in non-Hermitian quasicrystals, *Phys. Rev. Lett.* **129**, 113601 (2022).
- ¹¹⁰ S. Gandhi and J. N. Bandyopadhyay, Topological triple phase transition in non-Hermitian quasicrystals with complex asymmetric hopping, *Phys. Rev. B* **108**, 014204 (2023).
- ¹¹¹ S. Longhi, Phase transitions in non-Hermitian superlattices, *Phys. Rev. B* **107**, 134203 (2023).
- ¹¹² B. Midya, Topological phase transition in fluctuating imaginary gauge fields, *Phys. Rev. A* **109**, L061502 (2024).